Continuous reversal of Hanle resonances of a counter-propagating pulse and continuous-wave field

# Continuous reversal of Hanle resonances of a counter-propagating pulse and continuous-wave field

## Jelena Dimitrijević, Dušan Arsenović and Branislav M Jelenković

Institute of Physics, University of Belgrade, Pregrevica 118, 10080 Belgrade, Serbia

E-mail: jelena.dimitrijevic@ipb.ac.rs

## Abstract

In this work we study propagation dynamics of two counter-propagating lasers, a continuous-wave (CW) laser and the pulse of another laser, when both lasers are tuned to the $F_g = 2 \rightarrow F_e = 1$ transition in $^{87}$Rb, and can therefore develop Hanle electromagnetically induced transparency (EIT) in Rb vapor. We calculate the transmission of both lasers as a function of applied magnetic field, and investigate how the propagation of the pulse affects the transmission of the CW laser. Vice versa, we have found conditions when the Gaussian pulse can either pass unchanged, or be significantly absorbed in the vacuum Rb cell. This configuration is therefore suitable for convenient control of the pulse propagation and the system is of interest for optically switching the laser pulses. In terms of the corresponding shapes of the coherent Hanle resonances, this is equivalent to turning the coherent resonance from Hanle EIT into an electromagnetically induced absorption (EIA) peak. There is a range of intensities of both the CW laser and the laser pulse when strong drives of atomic coherences allow the two lasers to interact with each other through atomic coherence and can simultaneously reverse the signs of the Hanle resonances of both.

Keywords: electromagnetically induced transparency, electromagnetically induced absorption, pulse propagation

(Some figures may appear in colour only in the online journal)

## 1. Introduction

The interaction of atoms with lasers has been one of the most studied subjects during the past few decades. Coherent phenomena in atoms such as coherent population trapping [1], the Hanle effect [2] and related phenomena, electromagnetically induced transparency (EIT) [3] and electromagnetically induced absorption (EIA) [4] have been widely studied under various conditions. EIT and EIA can be induced in different atomic schemes. This can be a pump–probe configuration where two lasers couple two or more hyperfine (or Zeeman) levels. The other way to probe the distribution of atomic coherences is to apply a single optical field, while the transmission of the field is measured as a function of the magnetic field that varies the energy of Zeeman sublevels, so called Hanle configuration.

EIT and EIA narrow resonances and steep dispersion in the narrow spectral bandwidth of their resonances represent the unique properties of atomic systems. The ability to switch from EIT to EIA could provide a new technique to manipulate the properties of a medium. Yu *et al* [5] demonstrated transformation from the EIT to the EIA in the Hanle configuration when the polarization of a traveling wave changed gradually from linear to circular. This sign reversal was connected with the weak residual transverse magnetic field perpendicular to laser propagation. Bae *et al* [6] recently presented continuous control of the light group velocity from subluminal to superluminal propagation by using the standing-wave coupling field in the transition of the Λ-type

system of $^{87}$Rb atoms. When the coupling field changed from a traveling wave to a standing wave by changing the power of the counter-propagating laser field, the speed of the probe pulse changed from subluminal to superluminal propagation.

The counter-propagating geometry and the resulting variations of transmission and refractive index have also been explored. Chanu *et al* [7] recently showed that it is possible to reverse the sign of subnatural resonances in a (degenerate) three-level system. They observed the D2 line of Rb, in a room temperature vapor cell, and change was obtained by turning on a second control beam counter-propagating with respect to the first beam. The role of the different possible subsystems created in this configuration was analyzed [8], together with the possibility of tuning the strength of individual subsystems by changing the polarization of the control lasers.

Counter-propagation dynamics for the Hanle configuration has also been investigated [9–12]. Brazhnikov *et al* [11, 12] recently analyzed the counter-propagating geometry of two CW laser fields in the Hanle configuration. They used the polarization method to reverse the sign of the Hanle resonance of the CW field, and numerical and analytical calculations were performed for simple three-level schemes [11, 12].

In this paper, we present the development of Hanle resonances of two counter-propagating lasers, the CW and the Gaussian pulsed laser. Lasers having orthogonal linear polarizations both couple the $F_g = 2 \rightarrow F_e = 1$ transition in the $^{87}$Rb D1 line. Analysis is performed by numerically solving the set of Maxwell–Bloch equations for the same transition including all the magnetic sublevels and for the cold atoms. We have found a range of intensities for both lasers such that they can influence transmission of each other, that is, they can continuously reverse the sign of their resonances from EIT to EIA and *vice versa*, while the pulse is passing through the Rb cell. We are interested for dynamics in two special cases: when the pulse of one laser reverses the sign of the second, CW laser, and when both lasers can simultaneously switch each other's resonance signs.

## 2. Theoretical model

Here we describe the model that calculates the transmissions of two lasers which act simultaneously on Rb atoms. Namely, there is constant interaction with one laser, CW, and, at the same time, also with the pulse of the second laser. The set of Maxwell–Bloch equations (MBEs) is solved for all magnetic sublevels of the $F_g = 2 \rightarrow F_e = 1$ transition (see figure 1). From the optical Bloch equations (OBEs):

$$\frac{d\hat{\rho}(t)}{dt} = -\frac{i}{\hbar}[\hat{H}_0, \hat{\rho}(t)] - \frac{i}{\hbar}[\hat{H}_I, \hat{\rho}(t)] - \hat{SE}\hat{\rho}(t)$$
$$- \gamma\hat{\rho}(t) + \gamma\hat{\rho}_0 \qquad (1)$$

we calculate the evolution of density matrix $\hat{\rho}$. The diagonal elements of the density matrix, $\rho_{g_i,g_i}$ and $\rho_{e_i,e_i}$, are the populations, $\rho_{g_i,g_j}$ and $\rho_{e_i,e_j}$ are the Zeeman coherences, and $\rho_{g_i,e_j}$ and $\rho_{e_i,g_j}$ are the optical coherences. Here, indices g and e are for the ground and the excited levels, respectively.
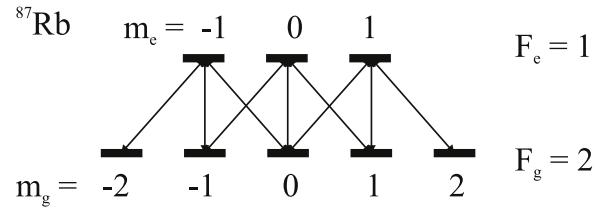


**Figure 1.** $F_g = 2$ and $F_e = 1$ hyperfine levels with the notation of magnetic sublevels.

MBEs are solved for the Hanle configuration, i.e. when the external magnetic field $B$ is varied around the zero value, as described by the Hamiltonian part $\hat{H}_0$. The direction of $\vec{B}$ is the direction of laser propagation and it is also the quantization axis. The Zeeman splitting of the magnetic sublevels is $E_{g(e)} = \mu_B l_{F_{g(e)}} m_{g(e)} B$, where $m_{g(e)}$ are the magnetic quantum numbers of the ground and excited levels, $\mu_B$ is the Bohr magneton and $l_{F_{g,e}}$ is the Landé gyromagnetic factor for the hyperfine levels. In equation (1), $\hat{SE}$ is the spontaneous emission operator, the rate of which is $\Gamma$, and in our calculations we have taken into account that the transition $F_g = 2 \rightarrow F_e = 1$ is open. The term $\gamma\hat{\rho}$ describes the relaxation of all density matrix elements, due to the finite time that an atom spends in the laser beam. The continuous flux of atoms entering the laser beams is described with the term $\gamma\hat{\rho}_0$. We assume equal populations of the ground Zeeman sublevels for these atoms. The role of the laser detuning (and Doppler broadening) is not discussed.

Atoms are interacting with the CW laser, and, for a limited time, they simultaneously also interact with another, pulsed laser. These interactions are described with Hamiltonian $\hat{H}_I$. The electric field vector represents the sum of two fields:

$$\vec{E}(t, z) = \sum_l [E_x^l \cos(\omega^l t - k^l z + \varphi_x^l)\vec{e}_x$$
$$+ E_y^l \cos(\omega^l t - k^l z + \varphi_y^l)\vec{e}_y]. \qquad (2)$$

In equation (2), $\omega^l > 0$ are the laser's (l) angular frequencies $\omega^l = \pm ck^l$, $k^l$ are wavevectors, where we take $k^l < 0$ when the propagation is in the negative direction of the $z$-axis, and $c$ is the speed of light. $E_x^l, E_y^l$ are the real Descartes components of amplitudes of the electric field while $\varphi_x^l, \varphi_y^l$ are associated phases and also real quantities.

We introduce the following substitution:

$$E_{++}^l = \frac{-E_x^l e^{+i\varphi_x^l} + iE_y^l e^{+i\varphi_y^l}}{2\sqrt{2}},$$

$$E_{+-}^l = \frac{-E_x^l e^{-i\varphi_x^l} + iE_y^l e^{-i\varphi_y^l}}{2\sqrt{2}},$$

$$E_{-+}^l = \frac{E_x^l e^{+i\varphi_x^l} + iE_y^l e^{+i\varphi_y^l}}{2\sqrt{2}}, \qquad (3)$$

$$E_{--}^l = \frac{E_x^l e^{-i\varphi_x^l} + iE_y^l e^{-i\varphi_y^l}}{2\sqrt{2}}.$$

With this substitution, the electric field vector stands:

$$\vec{E}(t, z) = \sum_l \vec{E}^l(t, z) \sum_l [e^{i(\omega^l t - k^l z)} \vec{u}_{+1} E^l_{++}$$
$$+ e^{i(\omega^l t - k^l z)} \vec{u}_{-1} E^l_{-+} + e^{-i(\omega^l t - k^l z)} \vec{u}_{+1} E^l_{+-}$$
$$+ e^{-i(\omega^l t - k^l z)} \vec{u}_{-1} E^l_{--}], \tag{4}$$

where $\vec{u}_{+1}$, $\vec{u}_{-1}$ and $\vec{u}_0$ are spherical unit vectors [13].

For the case of the two counter-propagating lasers that couple the same transition, we apply the multi-mode Floquet theory [14]. We use the approximation with the zeroth-order harmonics for the ground-state and excited-state density matrices, and up to the first-order harmonics for the optical coherences:

$$\rho_{g_i, e_j} = \sum_l e^{i(\omega^l t - k^l z)} \tilde{\rho}^l_{g_i, e_j},$$
$$\rho_{e_i, g_j} = \sum_l e^{-i(\omega^l t - k^l z)} \tilde{\rho}^l_{e_i, g_j}, \tag{5}$$

where the sum is taken over lasers that couple states $g_i$ and $e_j$.

The macroscopic polarization of the atomic medium $\vec{P}(t, z) = N_c e Tr[\hat{\rho}\hat{\vec{r}}]$ is calculated as

$$\vec{P}(t, z) = N_c \sum_l [e^{i(\omega^l t - k^l z)} (\vec{u}_{+1} P^l_{++} + \vec{u}_{-1} P^l_{-+})$$
$$+ e^{-i(\omega^l t - k^l z)} (\vec{u}_{+1} P^l_{+-} + \vec{u}_{-1} P^l_{--})], \tag{6}$$

where we introduced new quantities:

$$P^l_{++} = -\sum_{g_i \leftrightarrow e_j} \tilde{\rho}^l_{g_i, e_j} \mu_{e_j, g_i, -1},$$
$$P^l_{+-} = -\sum_{e_i \leftrightarrow g_j} \tilde{\rho}^l_{e_1, g_j} \mu_{g_i, e_j, -1},$$
$$P^l_{-+} = -\sum_{g_i \leftrightarrow e_j} \tilde{\rho}^l_{g_i, e_j} \mu_{e_j, g_i, +1},$$
$$P^l_{--} = -\sum_{e_i \leftrightarrow g_j} \tilde{\rho}^l_{e_i, g_j} \mu_{g_i, e_j, +1}. \tag{7}$$

The sum is taken over the dipole-allowed transitions induced by lasers (ls).

MBEs are solved for $E^l_{++}, E^l_{+-}, E^l_{-+}, E^l_{--}$ (given by equation (3)) which are complex amplitudes of the fields taking into account the relations $(E^l_{++})^* = -E^l_{--}$, $(E^l_{+-})^* = -E^l_{-+}$. MBEs for the propagation along the positive direction of the z-axis are

$$\left(\frac{\partial}{\partial z} + \frac{1}{c}\frac{\partial}{\partial t}\right) E^l_{++} = -i\frac{k^l N_c}{2\varepsilon_0} P^l_{++},$$
$$\left(\frac{\partial}{\partial z} + \frac{1}{c}\frac{\partial}{\partial t}\right) E^l_{-+} = -i\frac{k^l N_c}{2\varepsilon_0} P^l_{-+},$$
$$\left(\frac{\partial}{\partial z} + \frac{1}{c}\frac{\partial}{\partial t}\right) E^l_{+-} = +i\frac{k^l N_c}{2\varepsilon_0} P^l_{+-},$$
$$\left(\frac{\partial}{\partial z} + \frac{1}{c}\frac{\partial}{\partial t}\right) E^l_{--} = +i\frac{k^l N_c}{2\varepsilon_0} P^l_{--}, \tag{8}$$
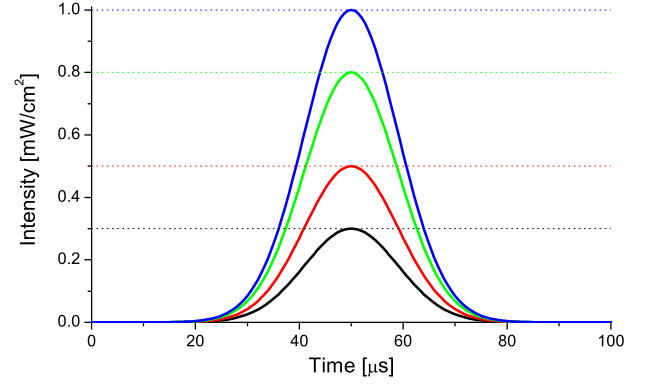


**Figure 2.** Figure shows the temporal waveforms of the laser amplitudes that we used in our calculations. The dashed lines indicate the amplitudes of the CW laser $I^0_{CW}$ and the solid lines are temporal waveforms of pulses $I_{pulse}$.

while those for the propagation along the negative direction of the z-axis are

$$\left(-\frac{\partial}{\partial z} + \frac{1}{c}\frac{\partial}{\partial t}\right) E^l_{++} = -i\frac{k^l N_c}{2\varepsilon_0} P^l_{++},$$
$$\left(-\frac{\partial}{\partial z} + \frac{1}{c}\frac{\partial}{\partial t}\right) E^l_{-+} = -i\frac{k^l N_c}{2\varepsilon_0} P^l_{-+},$$
$$\left(-\frac{\partial}{\partial z} + \frac{1}{c}\frac{\partial}{\partial t}\right) E^l_{+-} = i\frac{k^l N_c}{2\varepsilon_0} P^l_{+-},$$
$$\left(-\frac{\partial}{\partial z} + \frac{1}{c}\frac{\partial}{\partial t}\right) E^l_{--} = i\frac{k^l N_c}{2\varepsilon_0} P^l_{--}. \tag{9}$$

In the following text, we present results for the transmission of lasers, that is for the averaged power of the laser (l) electromagnetic fields:

$$I^l = c\varepsilon_0 \langle \vec{E}^l \cdot \vec{E}^l \rangle. \tag{10}$$

From equation (4) we have

$$I^l = c\varepsilon_0 \langle \{\vec{u}_{+1}[E^l_{++} e^{i(\omega^l t - k^l z)} + E^l_{+-} e^{-i(\omega^l t - k^l z)}]$$
$$+ \vec{u}_{-1}[E^l_{-+} e^{i(\omega^l t - k^l z)} + E^l_{--} e^{-i(\omega^l t - k^l z)}]\}^2 \rangle$$
$$= -2c\varepsilon_0 \{E^l_{++} E^l_{--} + E^l_{-+} E^l_{+-}\}. \tag{11}$$

## 3. Results and discussion

In this section we present effects on the Hanle EIT of the CW laser when the counter-propagating laser pulse, tuned to the same $F_g = 2 \rightarrow F_e = 1$ transition, passes the Rb cell, overlapping the CW laser. Conversely, we present results when the CW laser controls the transmission and the Hanle EIT of the laser pulse.

Transmissions of lasers are calculated for the values of the external magnetic field near zero, i.e. around the EIT resonance. Polarizations of both lasers are linear and orthogonal. We take the atom concentration in the cell $N_c = 10^{14}$ m$^{-3}$, the length of the cell is 10 cm, $\gamma = 0.001\,\Gamma$ and the spontaneous emission rate is $\Gamma = 2\pi\ 5.75$ MHz. The temporal shape of the laser pulse is Gaussian $I^0_{pulse} e^{-\frac{(t-t_0)^2}{\sigma^2}}$ (see figure 2), where $\sigma = 10\ \mu s/\sqrt{2\ln 2}$ and $I^0_{pulse}$ is the
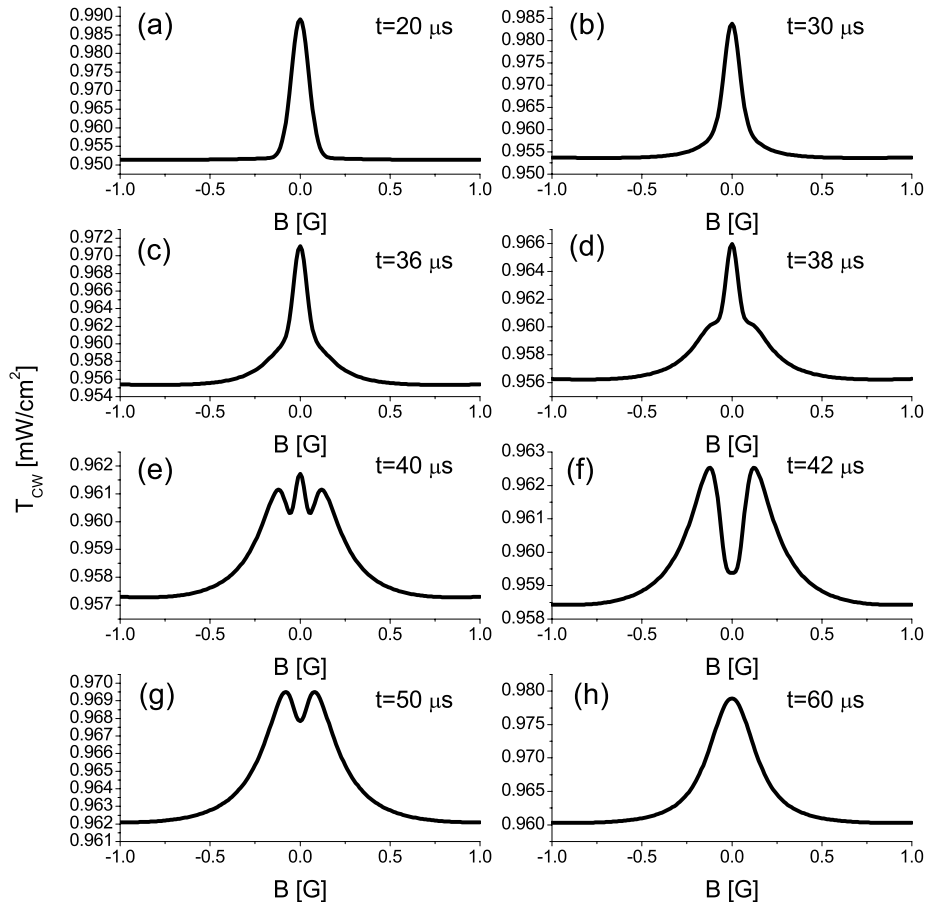
**Figure 3.** Transmission of the CW laser as a function of the magnetic field *B* at different times regarding the position of the pulse of the second laser with respect to the Rb cell: $t = 20$ μs (a), $t = 30$ μs (b), $t = 36$ μs (c), $t = 38$ μs (d), $t = 40$ μs (e), $t = 42$ μs (f), $t = 50$ μs (g) and $t = 60$ μs (h). The CW laser's intensity is $I_{CW}^0 = 1$ mW cm$^{-2}$ and the intensity of the pulse at the maximum is $I_{pulse}^0 = 0.3$ mW cm$^{-2}$ (solid black and dashed blue curves in figure 2). Note that the first curve is before the pulse even enters the cell, while curve (g) is at the time when the pulse is at the highest intensity, as can be seen from figure 2.

intensity of the laser pulse, at the peak of the amplitude at $t_0 = 50$ μs.

Since both lasers are resonant with the $F_g = 2 \rightarrow F_e = 1$ transition in $^{87}$Rb, each can independently induce EIT in the atomic vapor. As the pulse enters the cell, its intensity increases, reaches its maximal value $I_{pulse}^0$ and then decreases. At the very beginning of the pulse, atoms are interacting with the CW laser only, and the transmission of the CW field shows Hanle EIT. As the intensity of the pulse increases, atoms begin to interact with both superimposed fields. The resultant polarization, which is the sum of two orthogonal linear polarizations, can yield very different shapes of transmission resonances of both lasers.

As we see below, complete switching of the sign of the transmission resonance, from transmission gain to absorption gain, can happen depending on the ratio of the pulse's peak intensity $I_{pulse}^0$ and the intensity of the CW field $I_{CW}^0$. We will next discuss two possible cases, $I_{pulse}^0 < I_{CW}^0$ and $I_{pulse}^0 > I_{CW}^0$.

### 3.1. Hanle EIT resonances of the CW laser field in the presence of the weak laser pulse

In figure 3 we show changes of the CW laser Hanle EIT as the counter-propagating and spatially overlapping laser pulse

changes its intensity in the Rb cell. Results are for laser intensities $I_{CW}^0 = 1$ mW cm$^{-2}$ and $I_{pulse}^0 = 0.3$ mW cm$^{-2}$ (solid black and dashed blue lines in figure 2). As the laser pulse enters the cell the transmission of the CW laser still shows the Hanle EIT. Such is the case with the front of the pulse in the cell, that is for results presented in figures 3(a)–(c). As the pulse intensity increases, this EIT widens and structure begins to form at the resonance center. During the transient period, when the pulse intensity is increasing, there are instances when the CW transmission at the zero value of the external magnetic field totally switches its transmission behavior. Instead of the maximum transmission, when the laser pulse is off, it is maximally absorbed in the cell. It changes sign from EIT to EIA. With the back side of the pulse left in the cell, at time $t = 60$ μs, the transmission of the CW laser again shows EIT, and the resonance stays like this until there is no pulse laser in the cell.

For the choice of laser intensities considered here, $I \leq 1$ mW cm$^{-2}$, and with the condition $I_{pulse}^0 \leq I_{CW}^0$, the transmission of the pulse laser shows EIT at all times. Besides intensity broadening, the transmission of the pulse, as a function of the magnetic field, does not change significantly
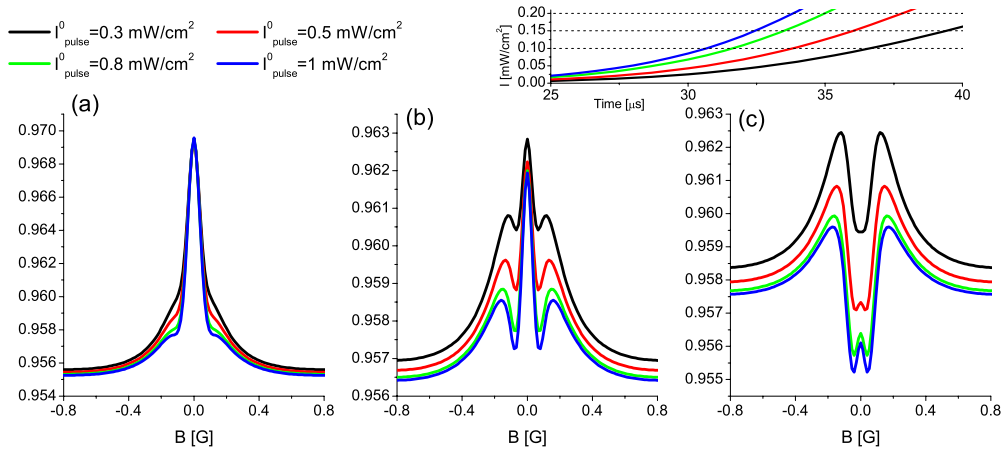
**Figure 4.** Transmissions of the CW laser for times when the pulse is entering the cell with three different intensities: $I_{pulse} = 0.1$ mW cm$^{-2}$ (a), $I_{pulse} = 0.15$ mW cm$^{-2}$ (b) and $I_{pulse} = 0.2$ mW cm$^{-2}$ (c). For each $I_{pulse}$ we present results for four different rise times of the intensity, i.e., when the pulse has maximum intensities $I_{pulse}^0 = 0.3$ mW cm$^{-2}$ (black curves), $I_{pulse}^0 = 0.5$ mW cm$^{-2}$ (red curves), $I_{pulse}^0 = 0.8$ mW cm$^{-2}$ (green curves) and $I_{pulse}^0 = 1$ mW cm$^{-2}$ (blue curves). The intensity of the CW laser is $I_{CW}^0 = 1$ mW cm$^{-2}$. The inset graph shows these three chosen intensities from four pulses as horizontal black dashed lines.
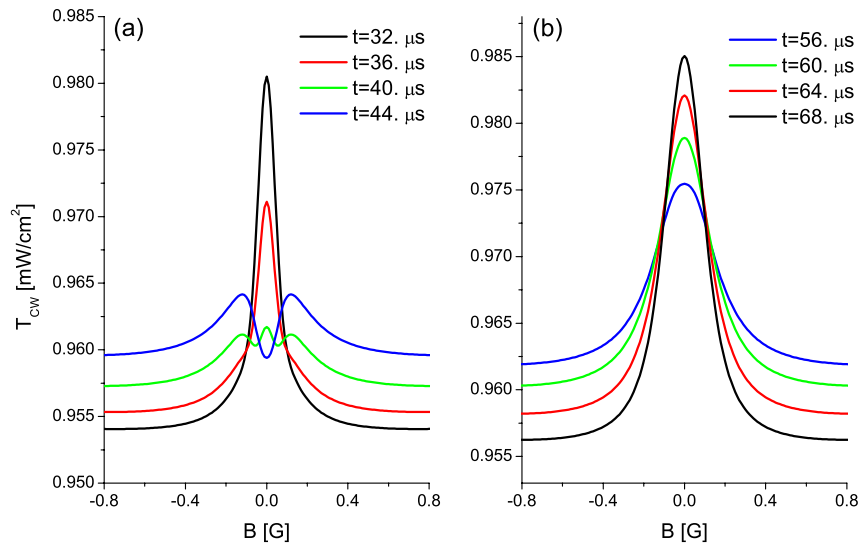


**Figure 5.** The transmissions of the CW laser, when the pulse laser takes four intensities from the rising (a) and falling (b) edges of the pulse. A certain intensity is chosen from the symmetrical moments of the pulse: $t = 32$ and $68$ $\mu$s (black curves), $t = 36$ and $64$ $\mu$s (red curves), $t = 40$ and $60$ $\mu$s (green curves) and $t = 44$ and $56$ $\mu$s (blue curves). The intensity of the CW laser is $I_{CW}^0 = 1$ mW cm$^{-2}$ and that of the pulse laser is $I_{pulse}^0 = 0.3$ mW cm$^{-2}$ (solid black and dashed blue curves in figure 2).

as the pulse passes. Results for the pulse's sign reversal are presented in section 3.2.

In figure 4 we compare the transmissions of the CW laser when four pulses, with different maximum values, have the same intensity in the cell: that is, when pulses whose maxima are $I_{pulse}^0 = 0.3$ mW cm$^{-2}$ (black curves), $I_{pulse}^0 = 0.5$ mW cm$^{-2}$ (red curves), $I_{pulse}^0 = 0.8$ mW cm$^{-2}$ (green curves) and $I_{pulse}^0 = 1$ mW cm$^{-2}$ (blue curves) (see figure 2), have the same values of $I_{pulse} = 0.1$ mW cm$^{-2}$ (a), $I_{pulse} = 0.15$ mW cm$^{-2}$ (b) and $I_{pulse} = 0.2$ mW cm$^{-2}$ (c).

Results in figure 4 show that, besides the intensity, the slope of the rising front of the pulse also determines the transmissions of the CW laser. Though atoms are affected by the same pulse intensity, as given in separate figures, the transmission of the CW field does not show identical

results when curves are compared. From figure 4 we see that evolution of the EIT/EIA passes through similar stages as the pulse rises, but the speed of the evolution of the EIT/EIA depends on the pulse's slope i.e. its first derivative. This also means that sign reversal of the CW laser, for different Gaussian pulses (different maximal intensities), does not happen simultaneously.

In figure 5 we show that the rising and falling edges of the laser pulses, with the same intensity, have different effects on the CW laser transmission. For the CW laser intensity of $I_{CW}^0 = 1$ mW cm$^{-2}$ and for the pulse laser maximum intensity of $I_{pulse}^0 = 0.3$ mW cm$^{-2}$, we present the CW laser transmission for four pairs of equal pulse laser intensity; each pair has the same intensity on both sides of the laser pulse. We choose the following pairs of intensities of the laser pulse,
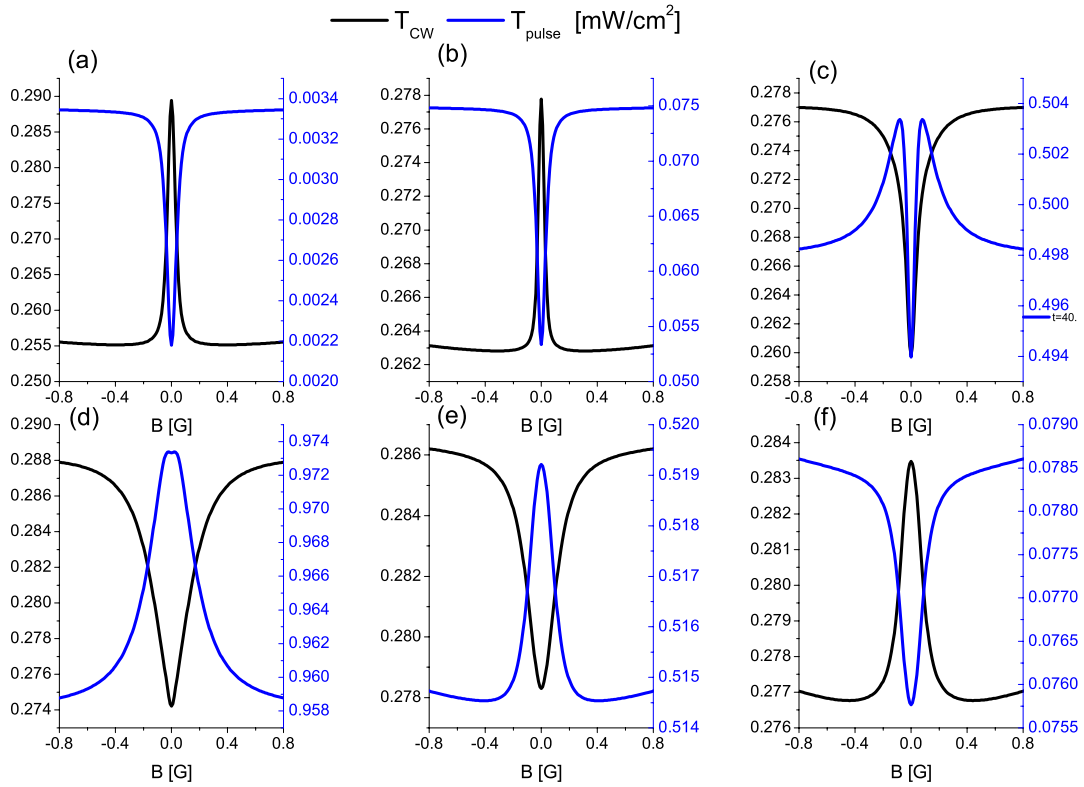
**Figure 6.** Transmissions of both the CW laser and the pulse as a function of the magnetic field: CW laser (black curves and black *y*-axis) and pulse laser (blue curves and blue *y*-axis). The amplitude of the CW laser's electric field is $I^0_{CW} = 0.3$ mW cm$^{-2}$ and the pulse's maximum value is $I^0_{pulse} = 1$ mW cm$^{-2}$ (solid blue and dashed black curves in figure 2). Results are presented for six values of the intensity of the Gaussian laser pulse as it passes through the cell, from $t = 20$ to $70$ $\mu$s in steps of $10$ $\mu$s: $t = 20$ $\mu$s (a), $t = 30$ $\mu$s (b), $t = 40$ $\mu$s (c), $t = 50$ $\mu$s (d), $t = 60$ $\mu$s (e) and $t = 70$ $\mu$s (f).

i.e., for the pulse instants $t = 32$ and $68$ $\mu$s (black curves), $t = 36$ and $64$ $\mu$s (red curves), $t = 40$ and $60$ $\mu$s (green curves) and $t = 44$ and $56$ $\mu$s (blue curves).

The results given in figure 5 indicate that the transmissions of the CW field are not symmetrical with respect to the pulse maximum intensity. Depending on whether the CW laser is overlapped with the rising (figure 5(a)) or the falling (figure 5(b)) edge of the pulse, the profiles have different waveforms, although the intensities are the same. A similar result of this 'memory effect' has also been discussed by Ignesti *et al* [15]. It was theoretically predicted that spectral enlargement or compression process occurs when the probe pulse is overlapped by a coupling pulse field with a positive or negative temporal slope, and experimental confirmation was obtained for a scheme in sodium atomic vapor [15]. At the rising edge of the pulse, while the dark-state is being formed, there are rapid changes in the transmission of the CW laser. The profiles at the falling edge of the pulse are due to long-lived ground-state coherences, created at the earlier time of the pulse propagation. After a certain time the dark-state is established and further decrease of the pulse's intensity does not affect the formed dark-state.

### 3.2. Switching signs of both laser transmissions

Our analysis indicates that the simultaneous switching of signs of transmission resonances of both CW and pulse laser

fields is when the intensity of the CW field is comparable to the pulse laser intensity, that is $I^0_{CW} \leq I^0_{pulse}$. For this ratio of intensities, when the pulse laser intensity after a certain time reaches the intensity of the CW laser, the intensities of the two lasers are comparable (see figure 2) and reversals of the signs of both are possible.

In figure 6 we present the transmissions of both lasers on the corresponding sides of the cell. For the case $I^0_{pulse} > I^0_{CW}$ (we analyzed range of intensities $I \leq 1$ mW cm$^{-2}$) both lasers are switching each other's resonance signs. The switching happens only at the time when the pulse intensity varies near its maximum; therefore, it is a very fast and short optical switch. Results in figures 6(d) and (e) show that both lasers have completely changed the sign of resonance from EIT/EIA to EIA/EIT. Results also show that there is a mirror symmetry between the transmission of the CW and pulse lasers. Both lasers change the sign of resonance simultaneously. The only exception to this is around $t = 40$ $\mu$s, when both lasers show EIA, when there are also most drastic changes in the evolution of the atomic ensemble.

We also calculated the transmission of the laser pulse for four values of the CW laser intensities. Results are given in figure 7 for $I^0_{CW} = 0.3$ mW cm$^{-2}$ (black curves), $I^0_{CW} = 0.5$ mW cm$^{-2}$ (red curves), $I^0_{CW} = 0.8$ mW cm$^{-2}$ (green curves) and $I^0_{CW} = 1$ mW cm$^{-2}$ (blue curves). The intensity of the pulse laser is $I^0_{pulse} = 1$ mW cm$^{-2}$. We observe the pulse's Hanle resonance in transmissions for three different
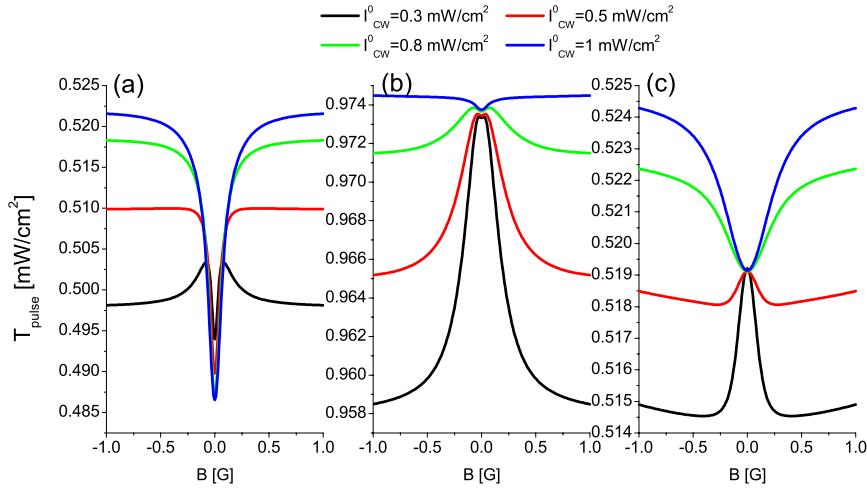
**Figure 7.** Transmissions of the pulse fields, when the CW laser takes different intensities: $I^0_{CW} = 0.3$ mW cm$^{-2}$ (black curves), $I^0_{CW} = 0.5$ mW cm$^{-2}$ (red curves), $I^0_{CW} = 0.8$ mW cm$^{-2}$ (green curves) and $I^0_{CW} = 1$ mW cm$^{-2}$ (blue curves). We observe transmissions at three different moments in time: $t = 40 \,\mu$s (a), $t = 50 \,\mu$s (b) and $t = 60 \,\mu$s (c). The maximum intensity of the pulse laser is kept constant, $I^0_{pulse} = 1$ mW cm$^{-2}$.
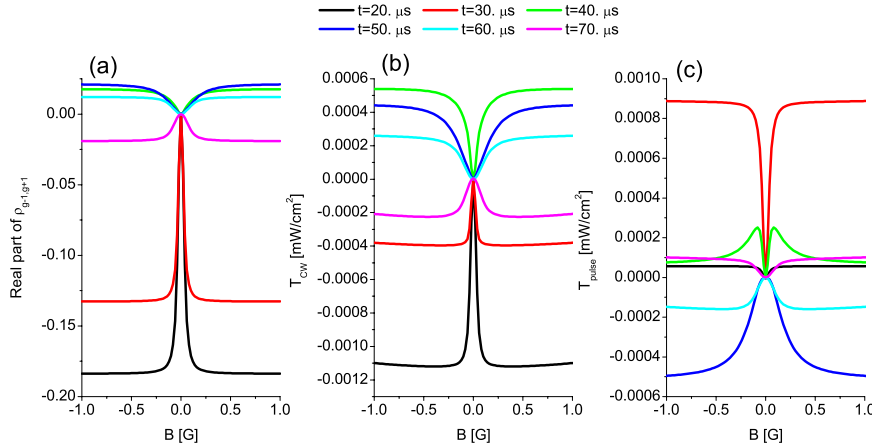


**Figure 8.** Real part of the ground-state coherences $\rho_{g_{-1,+1}}$ (a) and transmissions of the CW laser (b) and pulse laser (c) for six times during the time development of the pulse, from $t = 20$ to $70 \,\mu$s in steps of $10 \,\mu$s. Results for the coherences are calculated in the middle of the cell, $z = 0.05\ m$. The curves in all three graphs are $y$-shifted such that they coincide in $B = 0$.

times: $t = 40 \,\mu$s (a), $t = 50 \,\mu$s (b) and $t = 60 \,\mu$s (c). Results show that when the intensity of the CW field is varied, the transmission of the pulse laser at the zero magnetic field, for $B = 0$, remains constant at all times. The condition for CPT in the Hanle configuration is fulfilled at zero magnetic field, and is, in this case, well established by the pulse's stronger laser. As can be seen in figures 7(b) and (c), the rest of the pulse transmission profile, which violates the exact condition for the dark-state fulfilled at zero magnetic field, can show either EIT or EIA depending on the strength of the CW field intensity.

In figure 8 we present the real part of the ground-state coherences $\rho_{g_{-1,+1}}$ (a) and compare them with the transmissions of the CW laser (b) and pulse laser (c). Different colors indicate different intensities applied, i.e. different moments of the pulse propagation, from $t = 20$ to $70 \,\mu$s in steps of $10 \,\mu$s, whereas the intensity of the CW laser is constant, $I^0_{CW} = 0.3$ mW cm$^{-2}$. Curves in all three graphs are shifted along the $y$-axis for easier comparison. We present

results in the middle of the cell, since changes along the cell are negligible. In this configuration, the transmission of the CW laser matches the sign of the ground-state coherences, while that of the pulse laser is of the opposite sign. Results presented in figure 8 confirm that the behavior of the transmissions of both lasers closely follows the behavior of the ground-state coherences.

## 4. Conclusion

We have analyzed the propagation dynamics of two counter-propagating laser fields with Rb atoms in the Hanle configuration, one of which is a Gaussian pulse and the other is CW. We demonstrated continuous sign reversal of both lasers in the Hanle configuration. Sign reversal was obtained in two ways, of only the CW laser field and of both lasers. The choice lies in the ratio of the lasers' intensities. We have also analyzed peculiarities of these two cases, different slopes of pulses, the effect of different intensities and the behavior

of the ground-state coherences. The results obtained in this work may provide a useful reference for further research and interesting applications of EIT and EIA ultranarrow resonances.

## Acknowledgment

## References

[1]  Aspect A, Arimondo E, Kaiser R, Vansteenkiste N and Cohen-Tannoudji C 1988 *Phys. Rev. Lett.* **61** 826
[2]  Moruzzi G and Strumia F (ed) 1991 *The Hanle Effect and Level-Crossing Spectroscopy* (New York: Plenum) (Engl. transl.)
[3]  Arimondo E 1996 *Prog. Opt.* **35** 257
[4]  Akulshin A M, Barreiro S and Lezama A 1998 *Phys. Rev. A* **57** 2996
[5]  Yu Y J, Lee H J, Bae I H, Noh H R and Moon H S 2010 *Phys. Rev. A* **81** 023416
[6]  Bae I H and Moon H S 2011 *Phys. Rev. A* **83** 053806
[7]  Chanu S R, Pandey K and Natarajan V 2012 *Europhys. Lett.* **98** 44009
[8]  Pandey K 2013 *Phys. Rev. A* **87** 043838
[9]  Zibrov S A, Dudin Y O, Radnaev A G, Vassiliev V V, Velichansky V L, Brazhnikov D V, Taichenachev A V and Yudin V I 2007 *JETP Lett.* **85** 417
[10]  Zhukov A, Zibrov S A, Romanov G V, Dudin Y O, Vassiliev V V, Velichansky V L and Yakovlev V P 2009 *Phys. Rev. A* **80** 033830
[11]  Brazhnikov D V, Taichenachev A V, Tumaikin A M, Yudin V I, Ryabtsev I I and Entin V M 2010 *JETP Lett.* **91** 625
[12]  Brazhnikov D V, Taichenachev A V and Yudin V I 2011 *Eur. Phys. J.* D **63** 315
[13]  Edmonds A R 1974 *Angular Momentum in Quantum Mechanics* (Princeton, NJ: Princeton University Press)
[14]  Chu S I and Telnov D A 2004 *Phys. Rep.* **390** 1
[15]  Ignesti E, Buffa R, Fini L, Sali E, Tognetti M V and Cavalieri S 2011 *Phys. Rev. A* **83** 053411